



**HAL**  
open science

## **Sc-doped GeTe thin films prepared by radio-frequency magnetron sputtering**

Marek Bouška, Jan Gutwirth, Kamil Bečvář, Vladimír Kucek, Stanislav Slang, Petr Janíček, Lubomír Prokeš, Josef Havel, Virginie Nazabal, Petr Nemeč

### ► **To cite this version:**

Marek Bouška, Jan Gutwirth, Kamil Bečvář, Vladimír Kucek, Stanislav Slang, et al.. Sc-doped GeTe thin films prepared by radio-frequency magnetron sputtering. *Scientific Reports*, 2025, 15 (1), pp.627. <10.1038/s41598-024-84963-3>. <hal-04867555>

**HAL Id: hal-04867555**

**<https://hal.science/hal-04867555v1>**

Submitted on 6 Jan 2025

**HAL** is a multi-disciplinary open access archive for the deposit and dissemination of scientific research documents, whether they are published or not. The documents may come from teaching and research institutions in France or abroad, or from public or private research centers.

L'archive ouverte pluridisciplinaire **HAL**, est destinée au dépôt et à la diffusion de documents scientifiques de niveau recherche, publiés ou non, émanant des établissements d'enseignement et de recherche français ou étrangers, des laboratoires publics ou privés.



Distributed under a Creative Commons CC BY 4.0 - Attribution - International License



## OPEN Sc-doped GeTe thin films prepared by radio-frequency magnetron sputtering

Marek Bouška<sup>1</sup>, Jan Gutwirth<sup>1</sup>, Kamil Bečvář<sup>1</sup>, Vladimír Kucek<sup>2</sup>, Stanislav Šlang<sup>3</sup>, Petr Janíček<sup>3,4</sup>, Lubomír Prokeš<sup>5</sup>, Josef Havel<sup>5</sup>, Virginie Nazabal<sup>1,6</sup> & Petr Němec<sup>1</sup>✉

Radio frequency magnetron co-sputtering method employing GeTe and Sc targets was exploited for the deposition of Sc doped GeTe thin films. Different characterization techniques (scanning electron microscopy with energy-dispersive X-ray analysis, X-ray diffraction, atomic force microscopy, sheet resistance temperature-dependent measurements, variable angle spectroscopic ellipsometry, and laser ablation time-of-flight mass spectrometry) were used to evaluate the properties of as-deposited (amorphous) and annealed (crystalline) Ge-Te-Sc thin films. Prepared amorphous thin films have Ge<sub>48</sub>Te<sub>52</sub>, Ge<sub>46</sub>Te<sub>50</sub>Sc<sub>4</sub>, Ge<sub>44</sub>Te<sub>48</sub>Sc<sub>8</sub>, Ge<sub>43</sub>Te<sub>47</sub>Sc<sub>10</sub> and Ge<sub>41</sub>Te<sub>45</sub>Sc<sub>14</sub> chemical composition. The crystallization temperatures were found in the region of ~153–272 °C and they increase with scandium content. Upon amorphous-crystalline material phase change, large changes in sheet resistance were measured, with electrical contrast in terms of sheet resistance ratio  $R_{\text{annealed}}/R_{\text{as-deposited}}$  in the range of  $1.37 \cdot 10^{-4} - 9.1 \cdot 10^{-7}$ . Simultaneously, huge variations of optical functions were found as demonstrated by absolute values of optical contrast values (at 405 nm) in the range of  $|\Delta n| + |\Delta k| = 1.88 - 3.75$  reaching maximum for layer containing 8 at% of Sc.

**Keywords** Phase change materials, Scandium doping, Germanium telluride, Thin films

From the material science point of view, amorphous and crystalline chalcogenides are flexible inorganic, solid-state materials transparent in infrared spectral region. Their applications became involved in chemistry, biology, medicine, ecology, optics, photonics, electronics, and optoelectronics<sup>1–4</sup>. The unique optical properties of amorphous chalcogenides (wide transmission window, high linear- and non-linear index of refraction, and photosensitivity) make them very interesting for integrated optical devices. Specifically, in the field of research of tellurium-based chalcogenides and their thin films, reversible electrical switching phenomenon was first time reported by Ovshinsky<sup>5</sup>. In the end of 1980s and beginning of 1990s, phase change materials based on Ge-Sb-Te<sup>6</sup> and/or Ag-In-Sb-Te<sup>7</sup> systems have been discovered. The main scientific as well as technological interest of those tellurides is their ability to transform quickly and reversibly between amorphous and crystalline phases. Fast phase transformation can be induced reversibly through varying the electric field or temperature by heating via a laser pulse in optical recording applications<sup>8,9</sup>.

Modern applications which are considered for phase change materials contain non-volatile memories and more recently other photonic applications such as optical color rendering, nanopixel displays, reconfigurable nanoplasmonic devices, active terahertz photonics, metamaterials and metasurfaces, switchable modulators, etc<sup>10–13</sup>. It is worth noting importance and specificity of chemical bonding in chalcogenide phase change materials, which is discussed for example by Muller et al.<sup>14</sup> or Wuttig et al.<sup>15</sup>.

However, the chalcogenide thin films still need to be optimized and modified to obtain functional materials with improved properties. One of the possibilities is their doping with p- block and d-block elements<sup>16</sup> (for example sputtered Ge-Sb-Te materials doped with Al<sup>17,18</sup>, Ti<sup>19,20</sup>, Ni<sup>21</sup>, Cu<sup>22,23</sup>, Se<sup>24</sup>, Zr<sup>25</sup>, Sn<sup>26</sup>, Bi<sup>26</sup>, W<sup>27,28</sup>, Zn<sup>29</sup>, Cr<sup>30</sup> or Ru<sup>31</sup>). Recently, apart from above mentioned doping elements, the research is focused also on tellurium-based phase change materials doped by scandium. The basis for the idea of scandium doping comes from the

<sup>1</sup>Department of Graphic Arts and Photophysics, Faculty of Chemical Technology, University of Pardubice, Studentská 573, Pardubice 532 10, Czech Republic. <sup>2</sup>Department of General and Inorganic Chemistry, Faculty of Chemical Technology, University of Pardubice, Studentská 573, Pardubice 532 10, Czech Republic. <sup>3</sup>Center of Materials and Nanotechnologies, Faculty of Chemical Technology, University of Pardubice, nám. Čs. legií 565, Pardubice 530 02, Czech Republic. <sup>4</sup>Institute of Applied Physics and Mathematics, Faculty of Chemical Technology, University of Pardubice, Studentská 95, Pardubice 532 10, Czech Republic. <sup>5</sup>Department of Chemistry, Faculty of Science, Masaryk University, Kotlářská 2, Brno 611 37, Czech Republic. <sup>6</sup>ISCR (Institut des Sciences Chimiques de Rennes) – UMR 6226, CNRS, Univ. Rennes, Rennes F-35000, France. ✉email: petr.nemec@upce.cz

work of Rao et al. who showed by materials screening followed by experiments that Sc is one of the suitable candidates to improve the performance (crystallization kinetics) of phase change materials<sup>32</sup>. As of now, most of the investigations deal with the doping of  $\text{Sb}_2\text{Te}_3$  with Sc, while other phase change materials are studied rarely.

X. Chen et al. studied scandium doped antimony telluride for applications in both, reflective displays as well as ultrafast integrated photonic memory devices with very short erase and write speeds of 2 ns<sup>33</sup>. The fastest crystallization speed and improved data nonvolatility by tuning the composition in  $\text{Sc}_x\text{Sb}_2\text{Te}_3$  system was demonstrated for  $\text{Sc}_{0.3}\text{Sb}_2\text{Te}_3$ <sup>34</sup>. Furthermore, Sc doped  $\text{Sb}_2\text{Te}_3$  ( $\text{Sc}_{0.2}\text{Sb}_2\text{Te}_3$ ) allowing a writing speed of only 700 picoseconds without pre-programming has been described<sup>32</sup>. The study of underlying process of heterogenous nucleation revealed that heterogenous nuclei in  $\text{Sc}_x\text{Sb}_2\text{Te}_3$  are enriched Sc ~ 25 at% in core with ~ 1.0 nm size and  $\sim 10^{23}$ - $10^{24}$  m<sup>-3</sup> density<sup>35</sup>. Another recent work studied Sc doping in  $\text{Sc}_x\text{Sb}_2\text{Te}_3$  alloys from the point of view of reduced vacancy concentration, enhanced local rigidity, and elevated vacancy-diffusion barrier, which together retard the vacancy ordering which in turn might allow to engineer more robust resistance states in the crystalline  $\text{Sc}_{0.2}\text{Sb}_2\text{Te}_3$ <sup>36</sup>. All the thin films investigated in papers cited above were fabricated by magnetron (co-) sputtering. On the other hand, spin coating followed by annealing was successfully used for the preparation of Sc-Sb-Te thin films via molecular telluride inks<sup>37</sup>. It is worthy to note that Hu et al. employed high-throughput ab initio calculations to identify optimal dopants for  $\text{Sb}_2\text{Te}_3$  showing superior properties of Sc-doped material<sup>38</sup>. Computational techniques were also exploited to investigate bonding similarities and differences between yttrium and scandium doped  $\text{Sb}_2\text{Te}_3$ <sup>39</sup>. Moreover, Sc doping of another antimony telluride ( $\text{Sb}_2\text{Te}$ ) from the point of view of thermal stability and DFT calculations of the structure was reported<sup>40</sup>.

Regarding scandium doping of Ge-Sb-Te materials, thermal stability and operational speed of Sc doped  $\text{Ge}_2\text{Sb}_1\text{Te}_2$  prepared by radio-frequency (RF) magnetron sputtering was studied<sup>41</sup>. Finally, Sc doped  $\text{Ge}_2\text{Sb}_2\text{Te}_5$  has been shown as material for high-speed and low-power-consumption phase change memory<sup>42</sup>.

Contrary, to the best of our knowledge, no reports focused on scandium doping of Ge-Te materials were published yet. Therefore, to strengthen the knowledge of influence of Sc doping on the properties of phase change materials, this work is focused on the preparation and characterization of Sc doped GeTe thin films by RF magnetron co-sputtering. Indeed, fabricated films were characterized in as-deposited state (amorphous phase) as well as in crystalline state (after thermal annealing) using atomic force microscopy (AFM), scanning electron microscopy (SEM) with energy-dispersive X-ray analysis (EDS), X-ray diffraction (XRD), electrical resistivity, laser ablation time-of-flight mass spectrometry, and variable angle spectroscopic ellipsometry (VASE). The results indicate that maximal absolute optical contrast values  $|\Delta n|+|\Delta k|$  at blue wavelength are found for  $\text{Ge}_{44}\text{Te}_{48}\text{Sc}_8$  thin films.

## Methods, results and discussion

The RF magnetron co-sputtering of Ge-Te-Sc thin films was performed at a room temperature using the MPE600 multichamber deposition system (Plassys—Bestek, France). Two 50.8 mm targets with the composition of GeTe (99.999%) and Sc (99.99%) (ALB Materials, Inc., USA) were used. For the depositions, different RF powers were applied (power on Sc cathode [W]/power on GeTe cathode [W]). In detail, the RF power ratios used were as follows:  $\text{Ge}_{48}\text{Te}_{52}$  0/20;  $\text{Ge}_{46}\text{Te}_{50}\text{Sc}_4$  9/20;  $\text{Ge}_{44}\text{Te}_{48}\text{Sc}_8$  13/20;  $\text{Ge}_{43}\text{Te}_{47}\text{Sc}_{10}$  15/17;  $\text{Ge}_{41}\text{Te}_{45}\text{Sc}_{14}$  20/18. The power ratios were selected with the idea of doping of GeTe films with different content of Sc, ranging from 0 to approximately 15 at%. The depositions were performed at room temperature. The experimental conditions, held constant throughout all the depositions, were: background pressure  $\leq 5 \times 10^{-7}$  mbar, Ar working pressure  $5 \times 10^{-3}$  mbar, Ar flow rate 75 sscm, and target-to-substrate distance of about 8 cm with substrates rotation. Thin films were deposited on borosilicate glass and single crystalline silicon wafer (100) substrates. The deposition times (from 14 min 30 s to 18 min 15 s, depending on the composition) were adjusted to fabricate approximately 150 nm thick films, which is the thickness suitable for most of the experiments. To achieve desired thickness, experimental growth rates estimated for individual targets (i.e. GeTe and Sc) were used. Experimentally determined thicknesses of the thin films were in the range of 141–164 ( $\pm 2$ ) nm.

To study the effect of crystallization, as-deposited films were annealed in inert atmosphere (pure argon) at the temperature of 350 °C for 120 min (to assure that the crystallization proceeded) and slowly cooled down to room temperature.

The morphology and the chemical composition of films was checked by SEM (Tescan, VEGA 3, EasyProbe, Czech Republic). The EDS elemental composition data were obtained using a scanning electron microscope LYRA 3 (Tescan) equipped with EDS analyzer AZtec X-Max 20 (Oxford Instruments). The thin films deposited on silicon substrates were analyzed at 10 kV of acceleration voltage on five  $400 \times 400$   $\mu\text{m}$  areas. The EDS results were evaluated in AZtec software (Sc K $\alpha$ , Ge L $\alpha$ , Te L $\alpha$ ), averaged and error bars represent the standard deviation from averaged values. Atomic force microscopy (NT-MDT, Ntegra 2) was used to study topography of thin films within typical scanned area of  $5 \mu\text{m} \times 5 \mu\text{m}$ . The AFM scans were performed in the semi-contact mode (amplitude modulated AFM) using double-sided cantilever with the resonant frequency of 235 and 140 kHz ( $\pm 10\%$ ), respectively. The data were processed using Gwyddion software.

Sheet resistance temperature-dependent measurements were carried out in-situ using a 2-probe method with Pt wire contacts attached by a water-based colloidal graphite coating alongside the sample of 1 cm x 1 cm size, under argon atmosphere, measuring cell MHCS622E, Mikroptic (Netherlands). The heating rate was  $2^\circ\text{C min}^{-1}$ .

Optical functions (refractive indices (n) and extinction coefficients (k)) as well as thicknesses and band gap values of the thin films were determined by spectroscopic ellipsometry (VASE, J. A. Woollam Co., USA) within the spectral range of 300–2300 nm, measuring 100 revolutions with wave-lengths steps of 20 nm at selected angles of incidence (50°, 60° and 70°). Experimental data were analyzed using a three-layer model of optical functions: (i) the substrate (glass substrate), (ii) thin film, and (iii) the surface layer. For the analysis of as-deposited thin films' ellipsometric data, the Cody-Lorentz (C-L) model, which includes the suitable band edge function, the description of the weak Urbach absorption tail, as well as Lorentz oscillator, was applied<sup>43</sup>. This

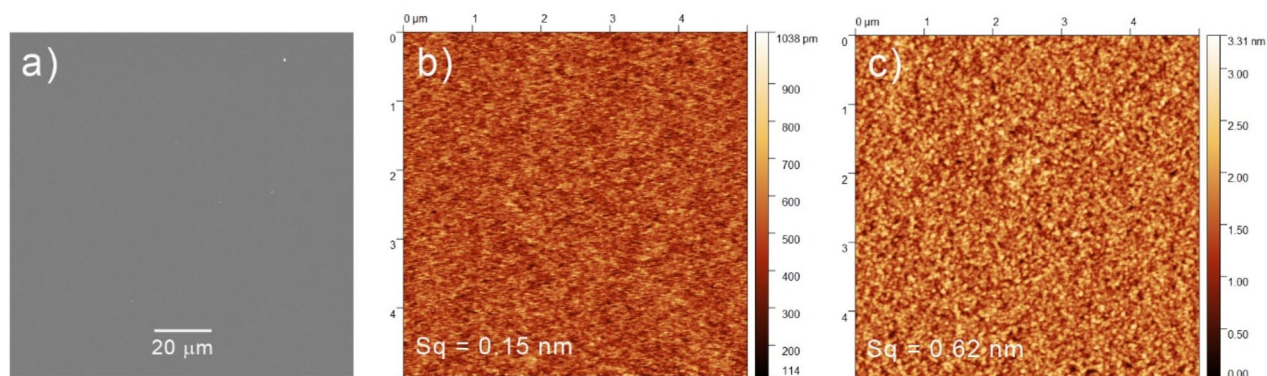


**Fig. 1.** SEM micrograph (a), AFM scan of (b) as-deposited and (c) annealed  $\text{Ge}_{44}\text{Te}_{48}\text{Sc}_8$  thin film ( $\text{Sq} \pm 0.1 \text{ nm}$ ).

Power Sc / GeTe [W/W]	a [Å]	V [Å <sup>3</sup> ]	Ge [at%]	Te [at%]	Sc [at%]	T <sub>c</sub> [°C]
0/20	5.920	207.475	48	52	0	153
9/20	5.936	209.154	46	50	4	207
13/20	5.944	209.987	44	48	8	211
15/17	5.944	209.987	43	47	10	249
20/18	NA	NA	41	45	14	272

**Table 1.** Lattice parameters of annealed Ge-Te-Sc thin films prepared at different sputtering power ratios: *a* is lattice parameter of GeTe cubic cell and *V* is volume of unit cell. Real chemical composition of prepared films (from EDS,  $\pm 1 \text{ at}\%$ ) is shown as well. Lattice parameters for the sample with highest content of sc are not available due to multiphase character of the sample (traces of tellurium and  $\text{Sc}_2\text{Te}_3$ ). Crystallization temperatures T<sub>c</sub> ( $\pm 2 \text{ }^\circ\text{C}$ ) determined from Rs temperature-dependent measurements.

model is appropriate for the description of amorphous chalcogenides' optical functions<sup>44,45</sup>. For the annealed layers, Drude-type contribution describing absorption of free carriers<sup>46</sup> was added to C-L model.

X-ray diffraction data were obtained with a D8-Advance diffractometer (Bruker AXS, Germany) with Bragg-Brentano  $\theta$ - $\theta$  geometry using CuK $\alpha$  radiation (40 kV, 30 mA) with a secondary graphite monochromator and equipped with Lynxeye XE-T detector. The diffraction angles were measured at room temperature from 5 to 60° (2 $\theta$ ) in 0.02° steps with a counting time of 1.5 s per step.

Mass spectra were acquired using an AXIMA Resonance hybrid quadrupole ion-trap time-of-flight mass spectrometer (Kratos Analytical Ltd., UK). The instrument was equipped with a nitrogen laser (337 nm). Measurements were performed in positive ion mode with a laser power ranging from 140 to 180 arbitrary units (a.u.) in the range of 90 to 850 m/z. For external calibration, red phosphorus clusters were utilized.

Thin films deposited by RF magnetron sputtering were amorphous and homogeneous. These characteristics were confirmed by room temperature XRD patterns and scanning electron microscopy images. The morphology of the layers is of good quality as exemplified by SEM (Fig. 1a) and AFM (Fig. 1b, c). Indeed, the SEM and AFM data showed smooth surface of thin films, without cracks or defects. For all amorphous thin films (exemplified by Fig. 1b), root mean square (RMS) surface roughness (Sq) values determined by AFM were typically found to be lower than  $\sim 0.4 \text{ nm}$ . On the other hand, Sq determined by AFM for crystallized layers (exemplified by Fig. 1c) was in the range of  $\sim 0.6$ – $1.3 \text{ nm}$ .

The chemical composition of fabricated thin films estimated by EDS is shown in Table 1. To study the effect of annealing, as-deposited films were annealed as specified above.

The crystallization temperatures T<sub>c</sub> were evaluated based on temperature dependences of thin films' sheet resistance (Rs) measurements upon heating as peaks of  $d(\ln R_s)/dT$  first derivatives. Electrical contrast in terms of sheet resistance ratio  $R_{s,\text{annealed}}/R_{s,\text{as-deposited}}$  was in the range  $1.37 \cdot 10^{-4}$  (for  $\text{Ge}_{46}\text{Te}_{50}\text{Sc}_4$ ) –  $9.1 \cdot 10^{-7}$  (for  $\text{Ge}_{48}\text{Te}_{52}$ ). The crystallization of the amorphous films was identified in the region of  $\sim 153$ – $272 \text{ }^\circ\text{C}$  (Table 1). This temperature range is common for GeTe<sup>47</sup> or scandium doped Ge-Sb-Te, Sb<sub>2</sub>Te or Sb<sub>2</sub>Te<sub>3</sub><sup>34,40–42</sup>. The former one is characterized by the very abrupt decrease of Rs (Fig. 2). It is important to mention that the crystallization temperature increases particularly with rising of scandium content. We note that for  $\text{Ge}_{46}\text{Te}_{50}\text{Sc}_4$ ,  $\text{Ge}_{43}\text{Te}_{47}\text{Sc}_{10}$ , and  $\text{Ge}_{41}\text{Te}_{45}\text{Sc}_{14}$  it is possible to observe second small drop in the R<sub>s</sub> temperature dependences (Fig. 2). One can hypothesize that this effect might be caused by structural transformation of Sc<sub>2</sub>Te<sub>3</sub> for which there are some

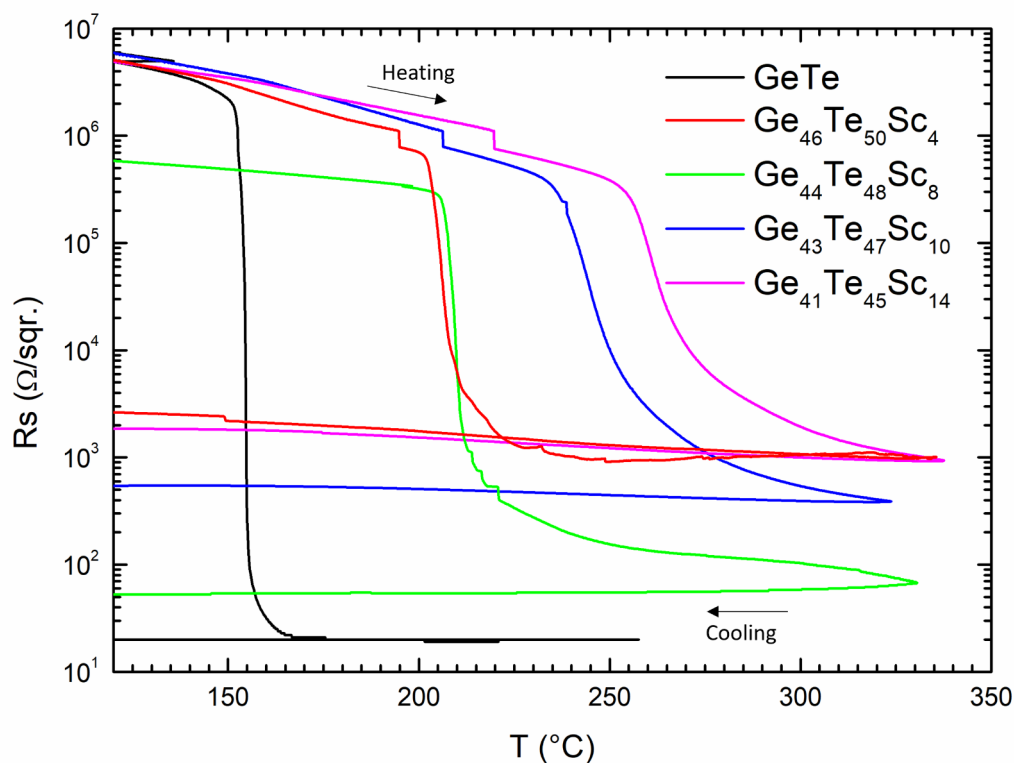


**Fig. 2.** Sheet resistance of as-deposited Ge-Te-Sc thin films (deposited on microscope glass substrates) upon heating followed by cooling.

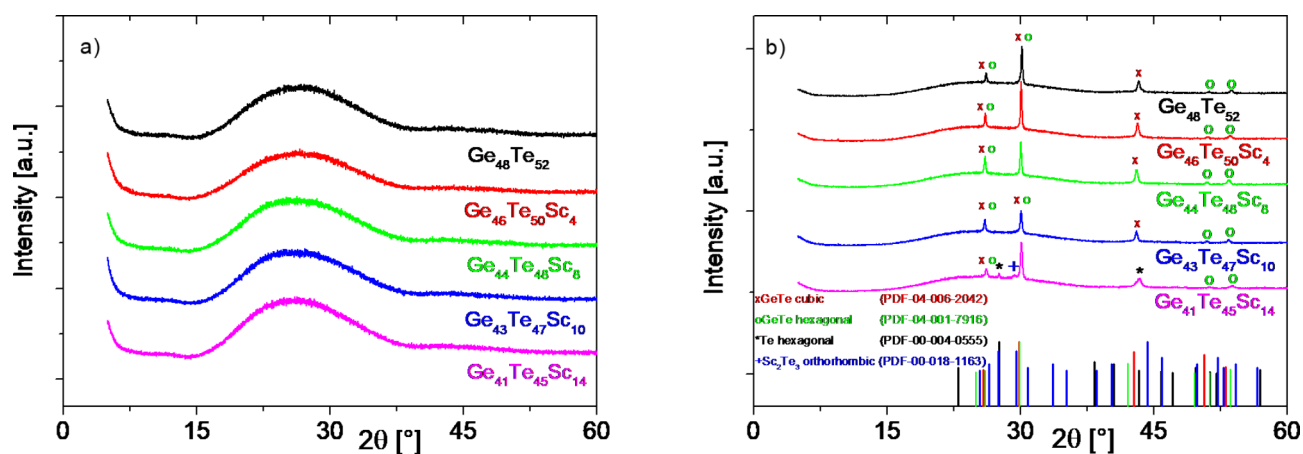


**Fig. 3.** XRD patterns of (a) as-deposited and (b) annealed Ge-Te-Sc thin films. The main phase in all annealed samples is cubic GeTe (PDF No. 04-006-2042). The traces of hexagonal GeTe, hexagonal Te and orthorhombic  $\text{Sc}_2\text{Te}_3$  phases are also indicated.

clues in the ab initio molecular dynamics simulations<sup>48</sup>. We would like to study this phenomenon in more detail in our future work.

XRD patterns of as-deposited films confirm their amorphous state (Fig. 3a). The lattice parameters and unit cell volume of annealed (crystalline) Ge-Te-Sc layers extracted from XRD patterns are summarized in the Table 1. From Table 1 is evident, that with increasing content of scandium, the lattice parameter  $a$  of cubic GeTe (main phase in the thin layers after the annealing) is increasing from 5.920 to 5.944 Å on rising Sc content up

to 8–10 at% of Sc. According to Vegard's law, this trend indicates the limit of solubility of Sc in GeTe matrix of approximately 10 at% of scandium. The increase of  $a$  parameter of GeTe upon increasing content of Sc is consistent with higher Shannon crystal (ionic) radii of Sc vs. Ge ( $r_c(\text{Ge}^{2+})=0.87 \text{ \AA}$  vs.  $r_c(\text{Sc}^{3+})=0.885 \text{ \AA}$  or  $r_t(\text{Ge}^{2+})=0.73 \text{ \AA}$  vs.  $r_t(\text{Sc}^{3+})=0.745 \text{ \AA}$ ; both for coordination number 6 in matrix of GeTe). Crystallized thin film with highest content of Sc (14 at%) contains apart from cubic GeTe also foreign phases: traces of tellurium and  $\text{Sc}_2\text{Te}_3$  as can be seen in Fig. 3b. The presence of hexagonal GeTe in crystallized Ge-Te-Sc thin films cannot be excluded as well (Fig. 3b).

Figure 4 illustrates the spectral dependencies of the optical functions (refractive indices ( $n$ ) and extinction coefficients ( $k$ )) for both as-deposited (top) and annealed (bottom) Ge-Te-Sc thin films. Although spectral dependences of optical functions are very similar for all samples in amorphous state one can notice slight increase in the refractive index (in the transparent part of spectra) and slight decrease of the onset of the absorption coefficient (energy bandgap) with the increasing content of Sc. It is worth to mention that spectral dependence of the refractive index and extinction coefficient of as-deposited as well as annealed GeTe film is in very good agreement with data reported earlier<sup>47,49</sup>. One can notice drastic change of the optical functions (both refractive index and extinction coefficient) induced by phase change (crystallization). Thicknesses of the films (as-deposited and annealed) and their surface roughnesses (modelled using Bruggeman type of effective medium approximation of void and material<sup>50</sup>) obtained by the best fit of the ellipsometry data are summarized in Table 2 together with parameter  $E_g$  of the C-L model (usually considered as optical band gap). Increase of surface roughness for annealed samples is consistent with the results from AFM. This observation was also reported earlier for Ge-Sb-Te films deposited by co-sputtering or pulsed laser deposition<sup>47,49</sup>. The decrease in thickness induced by crystallization, which is quantified by thickness ratio between amorphous and crystallized thin film (Table 2), is also typical for phase change memory materials and it was observed for example in<sup>47,49</sup>. Changes in  $E_g$  upon crystallization of Ge-Te-Sc thin films are of different sign (Table 2) depending on the chemical composition. In detail,  $E_g$  decreases upon crystallization for layers with lower Sc content (up to 8 at% of Sc) while for larger Sc concentration,  $E_g$  increases.

Optical contrast was calculated as  $\Delta n + i\Delta k$  ( $n, k$  (annealed)- $n, k$  (as-deposited)). The absolute values of optical contrast at 405 nm in terms of  $|\Delta n| + |\Delta k|$  can be found in Table 2. As reported previously<sup>47,49</sup> GeTe films deposited by magnetron sputtering exhibit drastic optical contrast 3.03 even higher than in case of commercial  $\text{Ge}_2\text{Sb}_2\text{Te}_5$  ( $\sim 2.25$ )<sup>51</sup>. Increase of the Sc content in the studied films clearly increases the value of the absolute optical contrast up to  $\sim 3.75$  for  $\text{Ge}_{44}\text{Te}_{48}\text{Sc}_8$  composition. Larger amount of Sc ( $> 8$  at%) then lowers the optical contrast (Table 2).

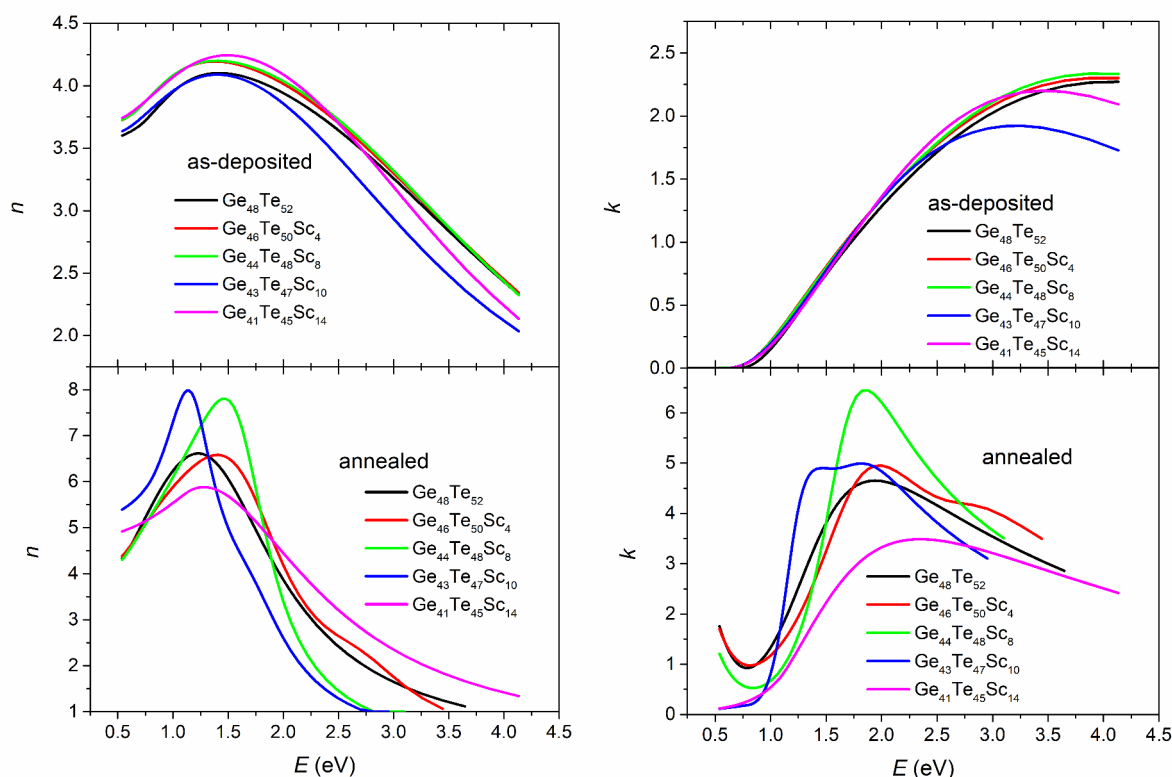


**Fig. 4.** Spectral dependences of refractive index (left) and extinction coefficient (right) of as-deposited (top) and annealed (bottom) Ge-Te-Sc thin films.

Sample	Thickness ratio as-dep/ann	Surface roughness as-dep/ann (nm)	Eg as-dep/ann (eV)	$ \Delta n + \Delta k $ (405 nm)
Ge <sub>48</sub> Te <sub>52</sub>	0.87	2/4	0.71/0.49	3.03
Ge <sub>46</sub> Te <sub>50</sub> Sc <sub>4</sub>	0.85	3/14	0.63/0.50	3.49
Ge <sub>44</sub> Te <sub>48</sub> Sc <sub>8</sub>	0.89	4/20	0.63/0.51	3.75
Ge <sub>43</sub> Te <sub>47</sub> Sc <sub>10</sub>	0.76	7/21	0.59/0.79	3.10
Ge <sub>41</sub> Te <sub>45</sub> Sc <sub>14</sub>	0.77	15/32	0.59/0.70	1.88

**Table 2.** Ge-Te-Sc thin films data obtained from spectroscopic ellipsometry analysis for amorphous (as-deposited) and crystallized (annealed) samples: thickness ratio ( $d \pm 2$  nm), surface roughness ( $\pm 1$  nm), optical band gap Eg ( $\pm 0.02$  eV), and absolute values of optical contrast  $|\Delta n|+|\Delta k|$  values at 405 nm ( $\pm 0.02$ ).

Finally, in the mass spectra, signals from Te and Ge-Te clusters predominated: Te<sup>2+</sup>, Te<sup>3+</sup>, Te<sup>4+</sup>, GeTe<sup>+</sup>, GeTe<sup>2+</sup>, and GeTe<sup>3+</sup>. Although oxidized species clusters were present, their intensity was low, indicating minimal surface oxidation of Ge-Te-Sc thin films.

## Conclusions

In conclusion, amorphous Ge-Te-Sc thin films with Sc content up to 14 at% were fabricated by RF magnetron co-sputtering. The quality of as-deposited (amorphous) and annealed (crystallized) layers was studied and the effect of scandium concentration on optical and electrical properties was monitored. Higher thermal stability and lower electrical contrast was observed with increasing scandium content. Regarding absolute optical contrast, increasing of Sc content in the studied films particularly increases its value up to  $\sim 3.75$  for Ge<sub>44</sub>Te<sub>48</sub>Sc<sub>8</sub>. Therefore, this particular composition could be of further interest for its detailed investigation and exploitation in the field of phase change memory materials.

## Data availability

The datasets used and/or analysed during the current study available from the corresponding author on reasonable request.

Received: 23 September 2024; Accepted: 30 December 2024

Published online: 03 January 2025

## References

1. Eggleton, B. J., Luther-Davies, B. & Richardson, K. Chalcogenide photonics. *Nat. Photonics* **5** (3), 141–148 (2011).
2. Adam, J. L. & Zhang, X. *Chalcogenide Glasses. Preparation, Properties and Applications* (Woodhead Publishing, 2014).
3. Noe, P., Vallee, C., Hippert, F., Fillot, F. & Raty, J. Y. Phase-change materials for non-volatile memory devices: from technological challenges to materials science issues. *Semicond. Sci. Technol.* **33** (1), 013002 (2018).
4. Blanc, W. et al. The past, present and future of photonic glasses: a review in homage to the United Nations International Year of glass 2022. *Progress Mater. Sci.* **134**, 101084 (2023).
5. Ovshinsky, S. R. Reversible electrical switching phenomena in disordered structures. *Phys. Rev. Lett.* **21**, 1450–1453 (1968).
6. Yamada, N., Ohno, E., Nishiuchi, K., Akahira, N. & Takao, M. Rapid-phase transitions of GeTe-Sb<sub>2</sub>Te<sub>3</sub> pseudobinary amorphous thin films for an optical disk memory. *J. Appl. Phys.* **69** (5), 2849–2856 (1991).
7. Iwasaki, H., Ide, Y., Harigaya, M., Kageyama, Y. & Fujimura, I. Completely erasable phase change Optical Disk, Japan. *J. Appl. Phys. Part. 1 - Regul. Papers Short. Notes Rev. Papers* **31** (2B), 461–465 (1992).
8. Raoux, S., Welnic, W. & Ielmini, D. Phase change materials and their application to nonvolatile Memories. *Chem. Rev.* **110** (1), 240–267 (2010).
9. Friedrich, I., Weidenhof, V., Njoroge, W., Franz, P. & Wuttig, M. Structural transformations of films studied by electrical resistance measurements. *J. Appl. Phys.* **87** (9), 4130–4134 (2000).
10. Wuttig, M., Bhaskaran, H. & Taubner, T. Phase-change materials for non-volatile photonic applications. *Nat. Photonics* **11** (8), 465–476 (2017).
11. Zhang, W., Mazzarello, R., Wuttig, M. & Ma, E. Designing crystallization in phase-change materials for universal memory and neuro-inspired computing. *Nat. Rev. Mater.* **4** (3), 150–168 (2019).
12. Gholipour, B. et al. Roadmap on Chalcogenide photonics. *J. Phys. Photonics* **5**, 012501 (2023).
13. Prabhathan, P. et al. Roadmap for phase change materials in photonics and beyond. *iScience* **26**, 107946 (2023).
14. Müller, P. C., Elliott, S. R., Dronskowski, R. & Jones, R. O. Chemical bonding in phase-change chalcogenides. *J. Phys. Condens. Matter.* **36**, 325706 (2024).
15. Wuttig, M. et al. Revisiting the nature of chemical bonding in chalcogenides to explain and design their properties. *Adv. Mater.* **35**, 2208485 (2023).
16. Bala, N. et al. Recent advances in doped Ge<sub>2</sub>Sb<sub>2</sub>Te<sub>5</sub> thin film based phase change memories. *Mater. Adv.* **4**, 747–768 (2023).
17. Sandhu, S., Kumar, S. & Thangaraj, R. Study of aluminium-modified Ge<sub>2</sub>Sb<sub>2</sub>Te<sub>5</sub> thin films for the applicability as phase-change storage device material. *Phase Trans.* **90**, 1013–1024 (2017).
18. Wang, G. et al. Improved thermal and electrical properties of Al-doped Ge<sub>2</sub>Sb<sub>2</sub>Te<sub>5</sub> films for phase-change random access memory. *J. Phys. D: Appl. Phys.* **45**, 375302 (2012).
19. Wei, S. J. et al. Phase change behavior in titanium-doped Ge<sub>2</sub>Sb<sub>2</sub>Te<sub>5</sub> films. *Appl. Phys. Lett.* **98**, 231910 (2011).
20. Park, J. & Bae, J. Effect of Ti diffusion on the microstructure of Ge<sub>2</sub>Sb<sub>2</sub>Te<sub>5</sub> in phase-change memory cell. *J. Electron. Microsc.* **64**, 381–386 (2015).
21. Zhu, Y. Q. et al. Ni-doped GST materials for high speed phase change memory applications. *Mater. Res. Bull.* **64**, 333–336 (2015).
22. Gao, Q. & Chen, L. Effect of Cu doping on microstructure and thermal stability of Ge<sub>2</sub>Sb<sub>2</sub>Te<sub>5</sub> thin film. *Appl. Phys. A* **125**, 564 (2019).
23. Ding, K. et al. Study on the Cu-doped Ge<sub>2</sub>Sb<sub>2</sub>Te<sub>5</sub> for low-power phase change memory. *Mater. Lett.* **125**, 143–146 (2014).

24. Buller, S. et al. Influence of partial substitution of Te by Se and Ge by Sn on the properties of the blu-ray phase-change material  $\text{Ge}_2\text{Sb}_2\text{Te}_{11}$ . *Chem. Mater.* **24**, 3582–3590 (2012).
25. Li, Z. G. et al. Changes in electrical and structural properties of phase-change Ge-Sb-Te films by Zr addition. *J. Non-Cryst Solids* **452**, 9–13 (2016).
26. Park, T. J., Choi, S. Y. & Kang, M. J. Phase transition characteristics of Bi/Sn doped  $\text{Ge}_2\text{Sb}_2\text{Te}_5$  thin film for PRAM application. *Thin Solid Films* **515**, 5049–5053 (2007).
27. Guo, P. et al. Sarangan, Tungsten-doped  $\text{Ge}_2\text{Sb}_2\text{Te}_5$  phase change material for highspeed optical switching devices. *Appl. Phys. Lett.* **116**, 131901 (2020).
28. Guo, S. et al. Temperature and concentration dependent crystallization behavior of  $\text{Ge}_2\text{Sb}_2\text{Te}_5$  phase change films: tungsten doping effects. *RSC Adv.* **4**, 57218–57222 (2014).
29. Wang, G. et al. Phase change behaviors of Zn-doped  $\text{Ge}_2\text{Sb}_2\text{Te}_5$  films. *Appl. Phys. Lett.* **101**, 051906 (2012).
30. Wang, Q. et al. Metal Doping of Phase Change materials: atomic arrangement of Cr-Doped  $\text{Ge}_2\text{Sb}_2\text{Te}_5$ . *J. Phys. Chem. C* **123**, 30640–30648 (2019).
31. Tan, Z. et al. Ruthenium doped  $\text{Ge}_2\text{Sb}_2\text{Te}_5$  nanomaterial as fast speed phase-change materials with good thermal stability. *Solid State Electron.* **186**, 108176 (2021).
32. Rao, F. et al. Reducing the stochasticity of crystal nucleation to enable subnanosecond memory writing. *Science* **358** (6369), 1423–1427 (2017).
33. Chen, X. et al. Neuromorphic photonic memory devices using ultrafast, non-volatile phase-change materials. *Adv. Mater.* **35**, 2203909 (2023).
34. Ding, K. et al. Recipe for ultrafast and persistent phase-change memory materials. *NPG Asia Mater.* **12**, 63 (2020).
35. Chen, B. et al. Insights into the heterogeneous nuclei of an ultrafast-crystallizing glassy solid. *Adv. Funct. Mater.* **34**, 2314565 (2024).
36. Song, T. et al. Metal–insulator transition in  $\text{Sc}_x\text{Sb}_y\text{Te}_3$  phase-change memory alloys. *Appl. Phys. Lett.* **124**, 062106 (2024).
37. Schenk, F. M. et al. Phase-change memory from molecular tellurides. *ACS Nano* **18**, 1063–1072 (2024).
38. Hu, S., Liu, B., Li, Z., Zhou, J. & Sun, Z. Identifying optimal dopants for  $\text{Sb}_2\text{Te}_3$  phase-change material by high-throughput ab initio calculations with experiments. *Comput. Mater. Sci.* **165**, 51–58 (2019).
39. Zhou, Y. et al. Bonding similarities and differences between Y–Sb–Te and Sc–Sb–Te phase-change memory materials. *J. Mater. Chem. C* **8**, 3646–3654 (2020).
40. Chen, X. et al. Scandium doping brings speed improvement in  $\text{Sb}_2\text{Te}_3$  alloy for phase change random access memory application. *Sci. Rep.* **8**, 6839 (2018).
41. Wang, Y. et al. High thermal stability and fast speed phase change memory by optimizing GeSbTe with scandium doping. *Scripta Mater.* **164**, 25–29 (2019).
42. Wang, Y. et al. Scandium doped  $\text{Ge}_2\text{Sb}_2\text{Te}_5$  for high-speed and low-power-consumption phase change memory. *Appl. Phys. Lett.* **112**, 133104 (2018).
43. Cody, G. D. (ed) *Jacques I. Pankove, in Semiconductors and Semimetals* 1st edn 11–82 (Academic, 1984).
44. Baudet, E. et al. Selenide sputtered films development for MIR environmental sensor. *Opt. Mater. Express* **6**, 2616 (2016).
45. Baudet, E. et al. Experimental design approach for deposition optimization of RF sputtered chalcogenide thin films devoted to environmental optical sensors. *Sci. Rep.* **7**, 3500 (2017).
46. Tiwald, T. E., Thompson, D. W., Woollam, J. A., Paulson, W. & Hance, R. Application of IR variable angle spectroscopic ellipsometry to the determination of free carrier concentration depth profiles. *Thin Solid Films* **313**, 661 (1998).
47. Bouska, M., Nazabal, V., Gutwirth, J., Halenkovic, T. & Nemeč, P. Radio-frequency magnetron co-sputtered Ge-Sb-Te phase change thin films. *J. Non-Cryst. Solids* **569**, 121003 (2021).
48. Zewdie, G. M., Debelab, T. T. & Asres, G. A. Effect of temperature on structural, dynamical, and electronic properties of  $\text{Sc}_2\text{Te}_3$  from first-principles calculations. *RSC Adv.* **12**, 32796 (2022).
49. Nemeč, P., Prikryl, J., Nazabal, V. & Frumar, M. Optical characteristics of pulsed laser deposited Ge–Sb–Te thin films studied by spectroscopic ellipsometry. *J. Appl. Phys.* **109**, 073520 (2011).
50. Bruggeman, D. A. G. Berechnung Verschiedener Physikalischer Konstanten Von Heterogenen Substanzen. I. Dielektrizitätskonstanten und Leitfähigkeiten Der Mischkörper Aus Isotropen Substanzen. *Ann. Phys.* **416**, 636–664 (1935).
51. Yamada, N. Origin, secret, and application of the ideal phase-change material GeSbTe. *Phys. Status Solidi B* **249**, 1837 (2012).

## Acknowledgements

Czech Science Foundation (22–07635S). Ministry of Education, Youth, and Sports of the Czech Republic, grant number LM2023037.

## Author contributions

M.B.: investigation, supervision, writing – original draft; J.G.: investigation; K.B.: investigation; V.K.: investigation; S.Š.: investigation; P.J.: investigation; L.P.: investigation; J.H.: investigation; V.N.: investigation, writing – review & editing; PN: conceptualization, methodology, supervision, funding acquisition, writing – review & editing.

## Declarations

## Competing interests

The authors declare no competing interests.

## Additional information

**Correspondence** and requests for materials should be addressed to P.N.

**Reprints and permissions information** is available at [www.nature.com/reprints](http://www.nature.com/reprints).

**Publisher's note** Springer Nature remains neutral with regard to jurisdictional claims in published maps and institutional affiliations.

**Open Access** This article is licensed under a Creative Commons Attribution-NonCommercial-NoDerivatives 4.0 International License, which permits any non-commercial use, sharing, distribution and reproduction in any medium or format, as long as you give appropriate credit to the original author(s) and the source, provide a link to the Creative Commons licence, and indicate if you modified the licensed material. You do not have permission under this licence to share adapted material derived from this article or parts of it. The images or other third party material in this article are included in the article's Creative Commons licence, unless indicated otherwise in a credit line to the material. If material is not included in the article's Creative Commons licence and your intended use is not permitted by statutory regulation or exceeds the permitted use, you will need to obtain permission directly from the copyright holder. To view a copy of this licence, visit <http://creativecommons.org/licenses/by-nc-nd/4.0/>.

© The Author(s) 2024